Journal of Solid State Chemistry **152,** 412–420 (2000)
doi:10.1006/jssc.2000.8698, available online at http://www.idealibrary.com on IDEAL®

Redox Behavior of VI B Transition Metal Ions in Rutile TiO_2 Solid Solutions: An XRD and EPR Study

Dante Cordischi,[1] Delia Gazzoli,* Manlio Occhiuzzi, and Mario Valigi

Centro SACSO (CNR), Dipartimento di Chimica, Università "La Sapienza," Piazzale Aldo Moro 5, Box 34-Roma 62, 00185 Roma, Italy; and
**Dipartimento di Ingegneria Meccanica e Industriale, Università Roma Tre, Via della Vasca Navale 79, 00146 Roma, Italy*

Received October 28, 1999; in revised form February 21, 2000; accepted March 3, 2000

CrO_2–TiO_2 (TC), MoO_2–TiO_2 (TMo), and WO_2–TiO_2 (TW), prepared by heating *in vacuo* at 1173–1273 K mixtures of MO_2 (M = Cr, Mo, or W) and TiO_2, were characterized by XRD and EPR. The transition metal ions were incorporated as isolated and clustered Cr^{III}, Mo^{IV}, and W^{IV} and a small fraction as isolated Mo^{V} and W^{V} in substitutional sites. After heating in air or in O_2 up to 1273 K, in TC no isolated Cr^{V} formed, whereas in TMo and TW, M^{IV} was oxidized to M^{V} and M^{VI}, and MO_3 was segregated. The oxidation started at 673 K and gave isolated substitutional Mo^{V} and isolated interstitial and substitutional W^{V}. After heating in H_2 up to 1073 K, TMo and TW reduction process differed: Mo^{IV} gave isolated and clustered Mo^{III}, and Mo^{IV}–Mo^{IV} pairs gave Mo_2^{7+} species; W^{IV} was not reduced to W^{III}; and temperatures > 900 K caused the segregation of metallic molybdenum and tungsten. © 2000 Academic Press

Key Words: **EPR; solid solutions; CrO_2–TiO_2; MoO_2–TiO_2; WO_2–TiO_2.**

INTRODUCTION

The oxides with rutile structure incorporate at impurity level a variety of cations with different ionic radius and charge. Solid solutions based on titanium dioxide have attracted much interest because in addition to their practical uses, their study has clarified concepts fundamental to solid state chemistry, including crystal growth and defect structure (1). It is often assumed that the incorporated guest species is randomly dispersed in the host lattice. This assumption is not valid when the guest ions having a suitable electronic configuration show metal–metal interactions.

In previous papers we studied the properties of VI B transition metal ions in rutile TiO_2 solid solutions and the experimental conditions required for their formations (2–5). When mixtures of MO_2 (M = Cr, Mo, or W) and TiO_2 were heated *in vacuo* at 1173–1273 K, solid solutions formed.

[1]To whom correspondence should be addressed. Fax: 39-6-490324. E-mail: cordischi@axrma.uniroma1.it.

Chromium entered into the rutile structure up to $\approx 4\%$ (Cr atoms/100 Ti atoms), as Cr^{III} ($3d^3$ ion). At higher chromium content compounds of general formula $Ti_{n-2}Cr_2O_{2n-1}$ were found. The treatment in air at 1273 K slightly decreased the solubility limit (3%) and changed the color (from orange to dark brown) because a non-stoichiometric compound, CrO_x, formed on the titania surface. The formation of this compound, revealed by XPS and optical diffuse reflectance in our laboratory (4), was confirmed by Ishida *et al*., using the same techniques (6). These investigators stated the probable value of x between 2.6 and 2.2. Molybdenum entered into the rutile structure up to $\approx 7\%$ and tungsten up to $\approx 5\%$. At a higher M content, MoO_2 or WO_2 and possibly metallic tungsten were present. In solid solutions most of molybdenum and tungsten were present as Mo^{IV} and W^{IV} (nd^2 ions), and electron paramagnetic resonance (EPR) identified a small fraction as Mo^{V} ($4d^1$ ion) (5).

The incorporation of Cr^{III}, Mo^{IV}, or W^{IV}, having an ionic radius larger than that of Ti^{IV}, causes an anisotropic expansion of the cell volume. Moreover, the pairing of the d electrons lowered the magnetic susceptibility. In CrO_2–TiO_2 and MoO_2–TiO_2, we found that specific magnetic susceptibility showed an antiferromagnetic Curie–Weiss behavior and magnetic moment, μ, decreased as the concentration of the incorporated ions increased. For the molybdenum-containing samples we measured μ values lower than the spin only value (1.8–2.1 vs 2.8 B.M.) (2). In WO_2–TiO_2, the specific magnetic susceptibility was practically coincident with that of undoped TiO_2 and independent of the W content (3).

In all these systems, X-ray diffraction (XRD) and magnetic measurements indicated metal–metal interactions along the c-axis of the rutile cell, in order to magnitude $W^{IV} > Mo^{IV} > Cr^{III}$, showing that VI B ions in rutile TiO_2 solid solutions are not randomly distributed.

In this study we reconsidered CrO_2–TiO_2, MoO_2–TiO_2, and WO_2–TiO_2 rutile solid solutions, to characterize the incorporated species better and to compare their stability in

0022-4596/00 $35.00

oxidizing and reducing atmospheres. For this purpose we used EPR spectroscopy and XRD measurements.

EXPERIMENTAL

Samples Preparation and Treatments

The samples were prepared as reported in detail elsewhere (2–4). Pelletted mixtures of MO_2 (M = Cr, Mo, W) and TiO_2 were heated at 1173–1223 K for 72–96 h in evacuated silica tubes. At the end of the thermal treatment, the silica tube was opened at room temperature (RT) and the pellets were thoroughly ground. To remove the molybdenum or the tungsten fraction present as separate phases (MoO_2 or WO_2 and possibly W), MoO_2–TiO_2 and WO_2–TiO_2 samples were leached. For leaching, the molybdenum-containing samples were treated with hot concentrated HNO_3 solution (≈ 9 M), and tungsten-containing samples first with aqua regia and then with NaOH 1 M. Both samples were then rinsed with distilled water and dried at 353 K for 24 h.

The CrO_2–TiO_2, MoO_2–TiO_2, and WO_2–TiO_2 samples are designated as TCx, TMox, and TWx (or $T^{53}Cx$, $T^{95}Mox$, and $T^{183}Wx$ when prepared using ^{53}Cr ($I = 3/2$), ^{95}Mo ($I = 5/2$), and ^{183}W ($I = 1/2$) enriched isotopes). The figure x gives the nominal M content (M atoms/100 Ti atoms), ranging from 0.05 to 5. The actual M content determined by atomic absorption spectroscopy was close to the nominal (2–4).

The TC samples were heated in air at 1273 K for 72 h. The TMo and TW samples were heated at increasing temperature in air or in dry O_2 (40 Torr) up to 1293 K for 5 h and in dry H_2 (40 Torr) up to 1273 K for 5 h. After the H_2 treatment, some TMo samples were heated in dry O_2 (40 Torr) up to 1073 K for 5 h. All thermal treatments with pure gasses were performed in a circulation all-glass apparatus equipped with a magnetically driven pump, a pressure transducer (MKS, Baratron), and a trap kept at 77 K and placed downstream from the silica reactor containing the specimen.

Characterization Techniques

XRD spectra were obtained on a Philips PW 1729 diffractometer by using a Debye-Sherrer camera, i.d. 114.6 mm. Unit cell parameters of TiO_2 were measured with Co$K\alpha$ (Fe-filtered) radiation. The estimated errors were $\pm 1 \times 10^{-4}$ Å in the cell parameter a_0, $\pm 2 \times 10^{-4}$ in the axial ratio $C = c_0/a_0$ and ± 0.02 Å^3 in the cell volume, $V = a_0^3 \times C$. Details of the cell parameter measurements are reported elsewhere (2–5). Cu–$K\alpha$ (Ni-filtered) radiation was used for phase analysis.

EPR spectra were recorded at RT, at 77 K, and occasionally at 4.2 K on a Varian E-9 spectrometer (X-band), equipped with an on-line computer for data processing. The absolute concentration of the paramagnetic species, N, was determined from the integrated area of the spectra, using $CuSO_4 \cdot 5H_2O$ and Cu(acac)$_2$, Cu-acetylacetonate, as standards by the equation

$$N_a = N_b \cdot \frac{g_b}{g_a} \frac{S_b(S_b + 1)}{S_a(S_a + 1)} \cdot \frac{A_a}{A_b}, \qquad [1]$$

where A are the integrated areas (measured at the same temperature), g the average g values, S the spin, and a refers to the sample and b to the standard (7). The g-values were determined using as reference the sharp peak at $g = 2.0008$ of the E_1' center (8) (marked with an asterisk in Figs. 3 and 8).

After thermal treatment in H_2 at $T \geq 773$ K, the spectral recording suffered from a decrease of the cavity quality factor, difficulty of tuning, and phase inversion. Moreover, signals due to partially reduced rutile were present: a sharp signal at $g = 2.00$ due to electron trapped probably on surface (9); an asymmetric signal at $g = 1.94$ assigned to Ti^{III} species (10–12); and a very broad band centered at $g \approx 2$, probably due to mobile paramagnetic defects. To avoid the difficulty of tuning and the phase inversion, we submitted the reduced samples to a subsequent treatment in O_2 (or in air) at 373 K. This treatment left the transition metal ion signals (see below) unchanged, but strongly decreased the matrix signals and restored the cavity quality factor. Finally, after thermal treatment in H_2 at $T \geq 1073$ K the formation of a metallic phase (Mo or W) rendered impossible the tuning of the EPR cavity.

RESULTS AND DISCUSSION

XRD Characterization

In TMo and TW samples, heating in air or in O_2 up to 1293 K caused cell parameter changes due to redox and segregation processes. The most concentrated samples (TMo5 and TW5) showed the largest changes (Table 1). For both the systems, starting from 973 K, the cell parameter, a_0, decreased, whereas the axial ratio, C, slightly increased. Consequently, the unit cell volume, V, remained constant up to 973 K and after heating at higher temperatures decreased, at 1273 K reaching the value of pure TiO_2 (Figs. 1a and 1b). The XRD powder patterns of these samples showed the MoO_3 or WO_3 reflections. The shrinkage of the unit cell volume suggests the oxidation of Mo^{IV} followed by the segregation of MoO_3.

Thermal treatments in H_2 up to 1073 K also changed TMo and TW cell parameters (Table 1). In TMo samples, temperatures up to 673 K left a_0 and C practically unchanged. At temperatures from 673 to 873 K, C slightly decreased, whereas a_0 markedly increased. At higher temperatures, a_0 sharply decreased and C increased, both

TABLE 1

Unit Cell Parameter a_0, Axial Ratio C, and Phase Analysis for TMo5 and TW5 Samples as a Function of Treatment Temperature in Air and in H_2

Sample	Treatment	T (K)	a_0 (Å)	C	Phases[a]
TMo5	air	298	4.6052	0.6417	R
		673	4.6052	0.6417	R
		773	4.6055	0.6421	R
		873	4.6051	0.6419	R
		973	4.6053	0.6417	R
		1073	4.5981	0.6430	R
		1173	4.5942	0.6441	R + MoO_3
		1273	4.5928	0.6441	R + MoO_3
		1293	4.5925	0.6441	R + MoO_3
TW5	air	298	4.6077	0.6414	R
		673	4.6079	0.6415	R
		773	4.6073	0.6415	R
		873	4.6079	0.6415	R
		973	4.6038	0.6423	R
		1073	4.6032	0.6427	R
		1273	4.5950	0.6439	R + WO_3
TMo5	H_2	298	4.6052	0.6417	R
		673	4.6049	0.6417	R
		773	4.6076	0.6413	R
		873	4.6121	0.6410	R
		973	4.6108	0.6414	R
		1073	4.5925	0.6444	R + Mo
TW5	H_2	298	4.6075	0.6414	R
		673	4.6060	0.6412	R
		873	4.6063	0.6414	R
		1073	4.5959	0.6424	R
		1273	4.5934	0.6437	R + W

[a] R = Rutile.

reaching the values of undoped TiO_2 ($a_0 = 4.5927$ Å and $C = 0.6441$). Consequently, at temperatures from ≈ 700 to ≈ 900 K, the unit cell volume, V, increased and then increasing the temperature decreased, at 1073 K reaching the value of undoped TiO_2 (Fig. 2a). The XRD pattern of these samples showed the reflections of metallic molybdenum. The expanding unit cell volume in the 700–900 K temperature range indicates the reduction of Mo^{IV} in solid solution to Mo^{III}, whereas the volume contraction observed at higher temperature arises from the segregation of metallic molybdenum. The formation of Mo^{III} is in agreement with the small variation of C, because the extra electron is located on an orbital not directed along the c-axis (2–4).

In TW samples, thermal treatments in H_2 up to 873 K left cell parameters substantially unchanged. At higher temperatures a_0 decreased and C increased, both tending to the values of undoped TiO_2. Consequently, at temperatures higher than 873 K the unit cell volume sharply decreased, at 1073 K reaching the value of pure TiO_2 (Fig. 2b). XRD revealed metallic tungsten as a separate phase. The sharp decrease in the unit cell volume is therefore caused by the reduction of W^{IV} to metallic tungsten, followed by segregation.

In undoped TiO_2, thermal treatment in H_2 up to 1073 K left unit cell parameters and volume practically unchanged (Fig. 2a).

EPR Characterization

The high sensitivity of the EPR spectroscopy allowed us to study dilute solid solutions (TC0.05, TMo0.1, and TW0.1), whose spectra were well resolved because of small dipolar interactions.

TC system. The dilute TC sample showed a complex spectrum with several lines extending over a large magnetic field interval, designated hereafter as signal A (Fig. 3) In the ^{53}Cr-enriched sample each component split into four lines

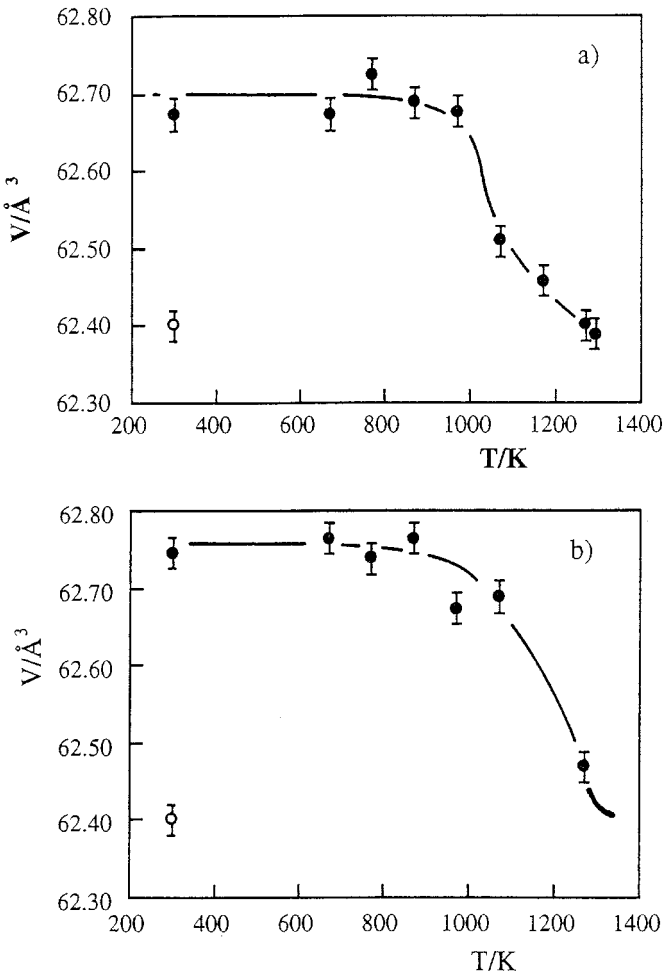

FIG. 1. Rutile unit cell volume, V, as function of the temperature of the treatment in air: (a) TMo5 (●) and TiO_2 (○); (b) TW5 (●) and TiO_2 (○).

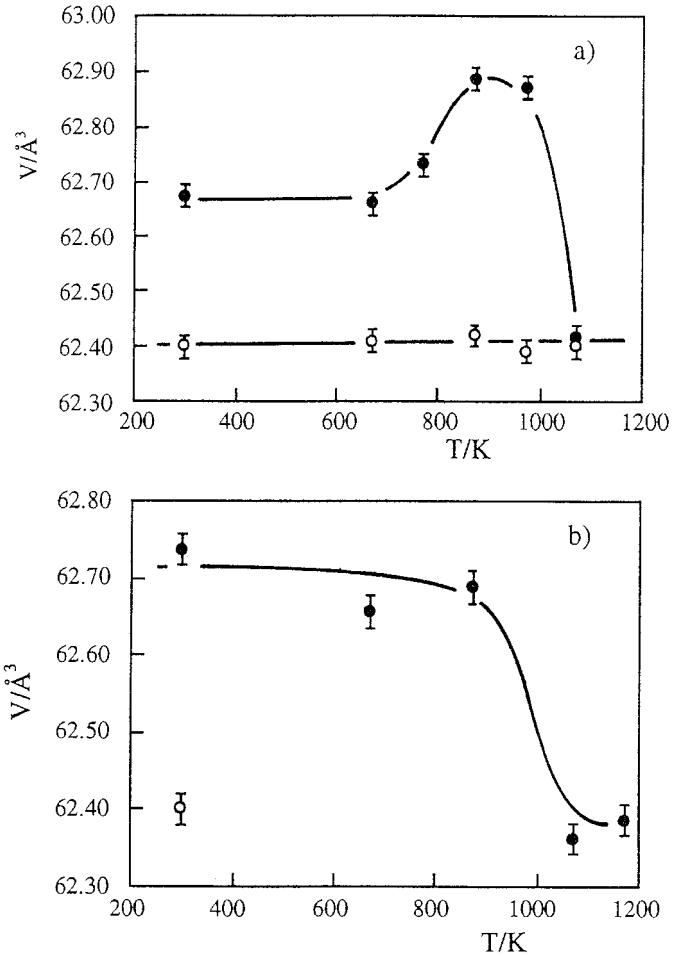

FIG. 2. Rutile unit cell volume, V, as function of the temperature of the treatment in H_2: (a) TMo5 (●) and TiO_2 (○); (b) TW5 (●) and TiO_2 (○).

(spectrum not shown). Similar signal has been detected in Cr-doped polycrystalline rutile and assigned to isolated Cr^{III} ions (6, 13, 14). The more concentrated samples, in addition to signal A, showed a broad ($\Delta H_{pp} \approx 1500$ G) band centered at $g \approx 2$ (signal B). As the Cr content increased, the B intensity increased and in TC5 accounted for a large fraction (if not all) of the analytical chromium. We therefore assigned signal B to clustered Cr^{III} ions (Fig. 3).

In all TC samples, thermal treatment in air at 1273 K left spectral features unchanged and slightly decreased the signal intensity. In particular, none of the TC samples showed signals due to Cr^{V} species. All attempts to generate Cr^{V} species in solid solution failed. EPR spectra of the dilute TC sample, pure or doped with the diamagnetic Ga^{III}-ion, recorded at RT, 77 and 4.2 K showed signal A alone.

Because Cr^{III} is difficult to reduce under the experimental conditions used here (15), we omitted the thermal treatments in H_2.

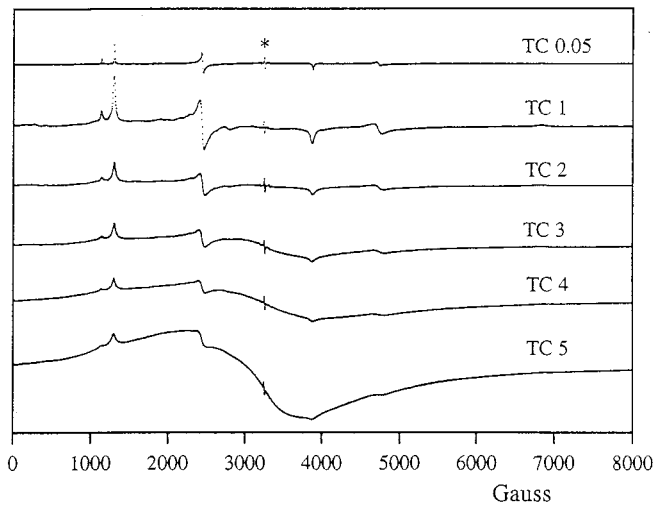

FIG. 3. EPR spectra at RT of TC samples. The spectra are normalized at the same gain. The asterisk indicates the marker at $g = 2.0008$.

TMo system. All EPR spectra of TMo samples recorded at 77 K showed a 3-g signal (Fig. 4a, signal C). In the ^{95}Mo-enriched samples each component of the **g** tensor split into six lines (Fig. 4c). The Spin-Hamiltonian parameters of signal C correspond, within the experimental error, to those of isolated Mo^{V} in the substitutional sites of

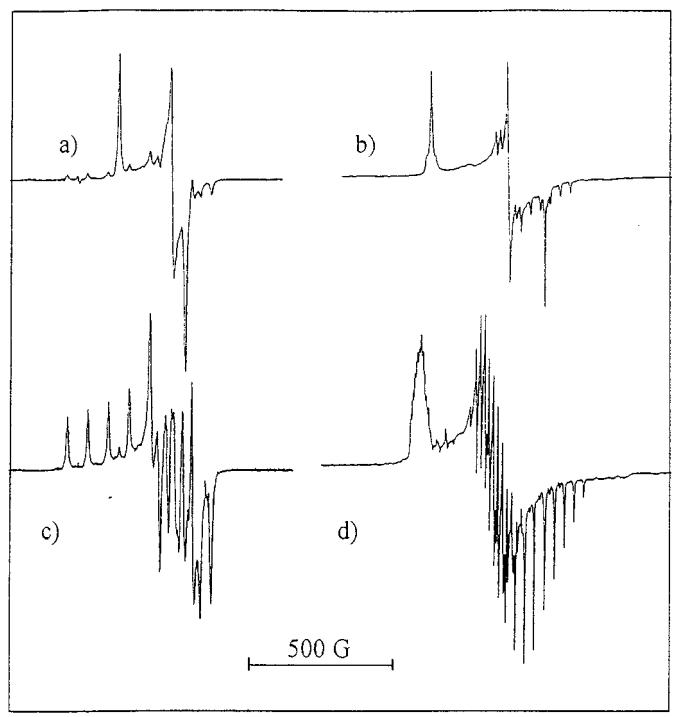

FIG. 4. EPR signals at 77 K of the following: TMo0.1 sample heated in O_2 at 1073 K (curve a); heated in H_2 at 1073 K (curve b); and T^{95}Mo0.1 sample heated in O_2 at 1073 K (curve c); heated in H_2 at 1073 K (curve d).

the rutile. This species has been identified in Mo-doped TiO_2 single crystals (16) and in MoO_2–TiO_2 polycrystalline samples (5, 17) (Table 2). The absolute concentration of Mo^V increased marginally with the total Mo content. Consequently, as the Mo content increased, the percentage of molybdenum detected by EPR as Mo^V markedly decreased ($\approx 15\%$ of the total molybdenum in TMo0.1 and $< 1\%$ in TMo5). Moreover, as the Mo-content increased, the signal C linewidth markedly increased (6 G in TMo0.1 and 20 G in TMo5).

The diluted samples (TMo0.1 and $T^{95}Mo0.1$) showed, together with C, two other signals. The first was a 3-g signal, typical of $S = 1/2$ species (Fig. 4b, signal D). In the ^{95}Mo-enriched samples each component split into 11 lines with a 1:2:3:4:5:6:5:4:3:2:1 intensity ratio (Fig. 4d). This pattern unambiguously indicates an interaction of the unpaired electron with two equivalent Mo nuclei. Hence we assign signal D to a dimeric Mo_2^{m+} species with an odd charge, m (delocalized mixed valence complex). The assignment of signal D to a dimeric species is in agreement with the average value (A_{av}) of the hyperfine constant, being about one half that of the mononuclear $S = 1/2$ species (Mo^V) (Table 2). The second signal shows several lines extending over a large magnetic field interval (Fig. 5, signal E). In the enriched samples each line split into a sextet (spectrum not shown). Analogously to the signal A in TC samples, we assign signal E in TMo to isolated Mo^{III} species ($4d^3$ ions, $S = 3/2$). The complex patterns of A and E signals arise essentially from the fine structure terms (D and E), the g factor of the nd^3 species in octahedral coordination being practically isotropic. To assign the resonance lines (Fig. 5) we used Van Reijen diagrams (18) and the Spin-Hamiltonian parameters from single crystal studies (19, 20).

As it did for the TMo0.1 sample, the leaching treatment left all EPR signals unchanged, indicating that the related species were in solid solution.

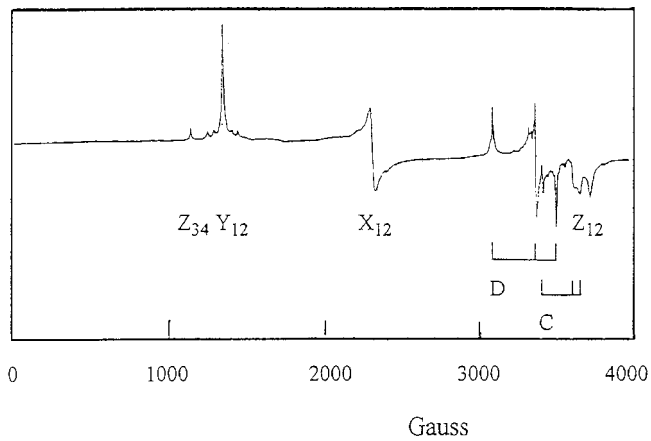

FIG. 5. EPR signals at 77 K of TMo0.1 untreated sample. Stick diagrams of signals C, D, and the assignment of the resonance lines of signal E are shown (the capital letters, X, Y, and Z, indicate the canonical orientations and the subscript numbers, 1–4, specify the spin levels in order of increasing energy).

In all TMo samples, thermal treatments in air (or in O_2) at $T > 573$ K caused D and E signals to disappear while the intensity of C progressively increased, reaching maximum at 1023–1073 K (Fig. 6). The maximum absolute concentration of Mo^V corresponded to about fivefold that assessed on untreated samples and was slightly dependent on Mo content ($\approx 0.06\%$ in TMo0.1 and $\approx 0.14\%$ in TMo5). Consequently, as the Mo content increased, the percentage of molybdenum detected by EPR as Mo^V markedly decreased ($\approx 60\%$ in TMo0.1 and $\approx 3\%$ in TMo5). Notably, after the thermal treatment in air at 1273 K, signal C remained intense. In TMo5 this treatment markedly sharpened the signal linewidth (9 G vs 20 G), whereas in TMo0.1 it left the linewidth unchanged (6 G).

In all TMo samples, heating in H_2 up to 573 K left EPR signals unchanged. At higher temperatures, D (Mo_2^{m+}) and

TABLE 2
EPR Parameters of d^1 Ions and of Dimeric Mo_2^{7+} Species in TiO_2 (Rutile)

Ion[a]	g_z	g_x	g_y	A_z[b]	A_x[b]	A_y[b]	g_{av}	Δg_{av}	A_{av}	Ref.
$V^{IV}_{(s)}$	1.9565	1.915	1.9135	142	31.5	43	1.9283	− 0.074	72.2	25
$Mo^{V}_{(s)}$	1.9167	1.8155	1.7923	65.7	24.7	30.8	1.8415	− 0.161	40.4	16
	1.916	1.815	1.791	65.3	25.4	30.1	1.841	− 0.162	40.3	This work
$W^{V}_{(s)}$	1.5944	1.4725	1.4431	92.5	40.8	63.7	1.5033	− 0.499	65.7	21
	1.594	1.473	1.443	92.0	41.1	63.8	1.503	− 0.499	65.6	This work
$V^{IV}_{(i)}$	1.9407	1.9865	1.9930	111.4	45.4	60.5	1.9734	− 0.029	72.4	24
$Mo^{V}_{(i)}$	1.857	1.897	1.920	58.5	32.7	51.2	1.891	− 0.111	47.5	26
$W^{V}_{(i)}$	1.673	1.735	1.795	50.8	39.8	87.2	1.734	− 0.268	59.3	This work
Mo_2^{7+}	2.113	1.939	1.867	6.9	15.7	29.6	1.973	− 0.029	17.4	This work

[a] The figure (s) indicates substitutional and (i) interstitial species.
[b] The hyperfine constants are expressed in 10^{-4} cm^{-1}.

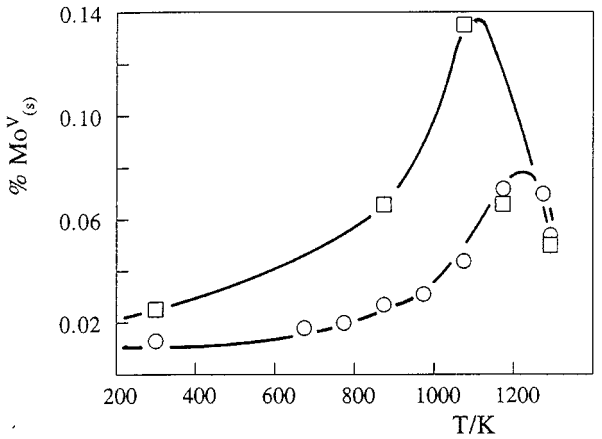

FIG. 6. Absolute concentration (atomic%) of Mo^{V} substitutional ions detected by EPR as function of the temperature of the treatment in air: TMo0.1 (○), and TMo5 (□).

E (Mo^{III}) signals progressively increased and at 873 K, C (Mo^{V}) disappeared. On subsequent treatment in O_2 at increasing temperatures, heating at 873 K destroyed D and E and restored C. At 1073 K the intensity of C markedly exceeded its initial value (Fig. 7). These results indicate that signals D and E both originate from reduced molybdenum species. Hence the dimeric Mo_2^{m+} species probably has an m value of 7. Interestingly, a Ti_2^{7+} species (not EPR-detectable at RT), with g values close to that of Ti^{III} species, has been found in the Magnéli phases of oxygen-deficient rutile (10, 11).

TW system. All EPR spectra of TW samples recorded at 77 K showed a rather weak 3-g signal (Fig. 8a, signal F). Its Spin-Hamiltonian parameters correspond, within the experimental error, to those of isolated W^{V} in the substitutional sites of rutile, detected in W-doped TiO_2 single crystals (21) (Table 2). Similar signals have also been detected in Mo and W-doped SnO_2 and GeO_2 and assigned to Mo^{V} and W^{V} in the substitutional sites of these rutile-like matrices (22, 23).

The samples heated in air at $T \geq 673$ K showed, together with signal F, another 3-g signal (Fig. 8a, signal G). Neither signal was detected at RT. In the ^{183}W-enriched samples each component of the **g** tensor split into a doublet (Fig. 8b). Hence, both signals originate from paramagnetic species interacting with a single W nucleus.

The rutile structure, besides the normal cationic sites containing Ti^{IV} ions, contains unoccupied interstitial sites having the same arrangement of surrounding anions and the same local symmetry (D_{2h}) (24). The most important difference is that the six nearest O^{2-} anions are arranged in the substitutional site as an elongated octahedron and in the interstitial site as a flattened octahedron. The nd^1 ions can occupy the substitutional (16,17,25) and the interstitial site, as does V^{IV} in TiO_2 single crystal (24) and Mo^{V} in polycrystalline titania (26). Theoretical arguments (27, 28) give the energy levels ordering of a nd^1 ion located in an elongated or flattened octahedron, from which the expected order of magnitude for the g-values is: $g_z > g_x > g_y$ for a substitutional ion and $g_z < g_x < g_y$ for an interstitial ion. Because F and G signals both originate from mononuclear W^{V} species, we assign the signal G to W^{V} ions in the interstitial sites of TiO_2 by analogy with V^{IV} and Mo^{V}. Another argument in favor of this assignment arises from the comparison of the average values of **g** and **A** tensors (g_{av} and A_{av}) in V^{IV}, Mo^{V}, and W^{V}, listed in Table 2. For each nd^1 ion, A_{av} is about the same in both sites, whereas g_{av} is markedly different. The g_{av} deviation from the spin only value ($\Delta g_{av} = g_{av} - g_e$) for the substitutional site is about twice as great as that for the interstitial site (Table 2). This regularity supports the assignment of signal G to W^{V} ions in the interstitial sites of rutile. The equations generally used to relate the EPR parameters of the nd^1 ions to the electronic

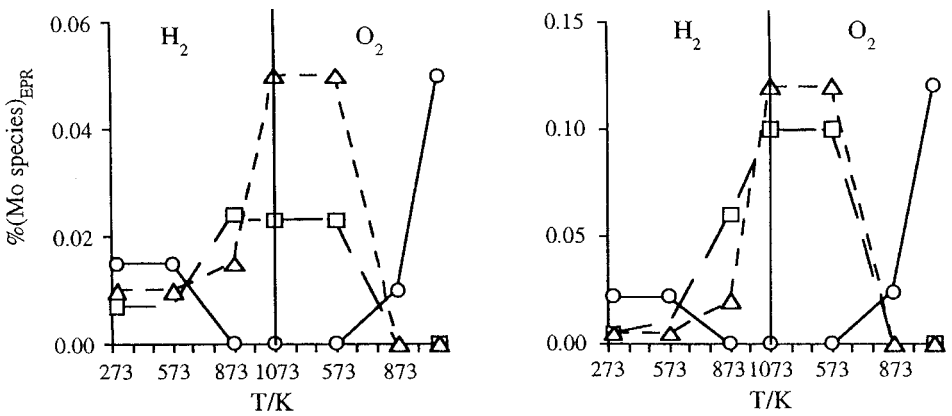

FIG. 7. Absolute concentration of molybdenum species (at.%) detected by EPR as function of the temperature of the treatment in H_2. (Left) TMo0.1, (right) TMo0.5: (○) isolated substitutional Mo^{V} ions (signal C), (□) dinuclear Mo_2^{7+} species (signal D), (△) isolated Mo^{III} ions (signal E).

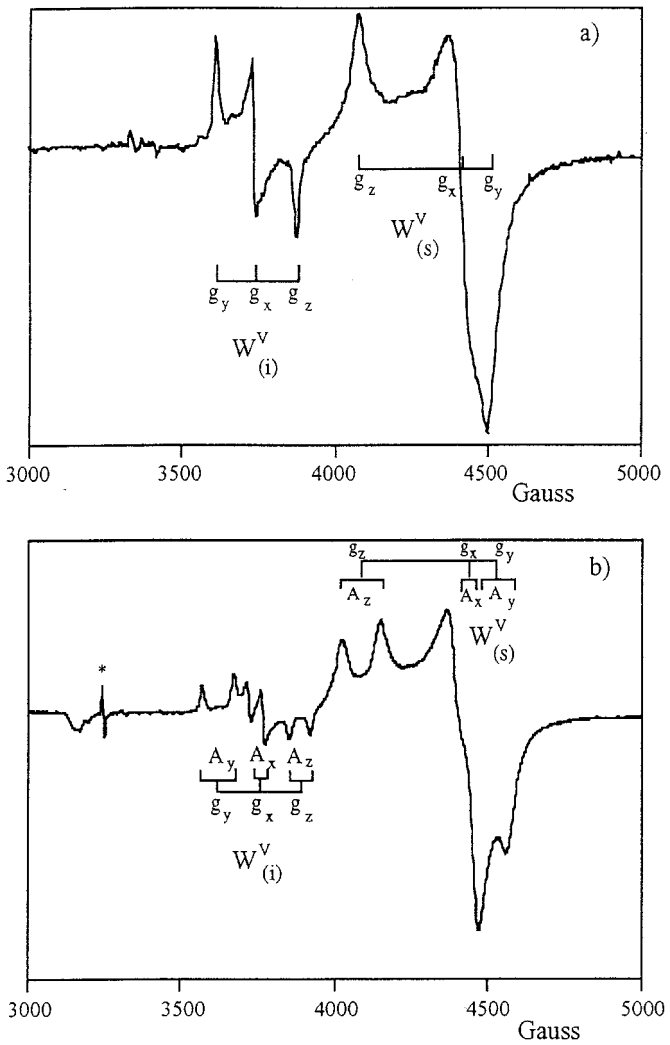

FIG. 8. EPR spectra at 77 K of TW1 sample (a) and $T^{183}W0.1$ sample (b) heated in air at 1073 K. The asterisk indicates the marker at $g = 2.0008$.

wave function of the ground state and to the energy levels of excited states are based on the second-order perturbation theory (29–31). These equations cannot be applied to W^V, because its spin-orbit coupling constant ($\sim 5000\ cm^{-1}$ (22)) is of the same magnitude as the crystal field. On the other hand, more complex molecular orbital calculations, taking into account the covalence (22, 30, 31), introduce a number of unknown quantities greater than the number of experimental EPR parameters. Therefore, without additional experimental data (f.i. energy levels from electronic spectra), these equations cannot be used here.

In all TW samples, after thermal treatment in air the signal G formed at 673 K, F and G intensities increased, reaching a maximum at 873 K, and sharply decreased at higher temperatures. Both signals disappeared at 1073 K (Fig. 9). The absolute concentration of both species was independent of the total W content. Consequently, as the W content increased, the percentage of tungsten detected by EPR as W^V markedly decreased ($\approx 30\%$ of the total tungsten in TW0.1 and $< 1\%$ in TW5).

In all TW samples, thermal treatments in H_2 at $T > 573$ K caused a continuous decrease in signal F intensity. EPR detected no signal attributable to other W species.

Comparison between TC, TMo, and TW Systems

The thermal treatment of TC in oxidizing atmosphere up to 1273 K failed to induce the formation of isolated Cr^V ions in solid solution. Cr^V as chromyl ion with a square pyramidal configuration has been detected at RT on the surface of various oxides, including TiO_2 (32). Cr^V in tetrahedral coordination has been detected at $T \leq 77$ K on silica surface (32, 33), in Cr-doped phosphates (34, 35) and in irradiated Cr-doped sulfates (36). Isolated Cr^V in a distorted octahedral configuration has been found in $SrTiO_3$ after

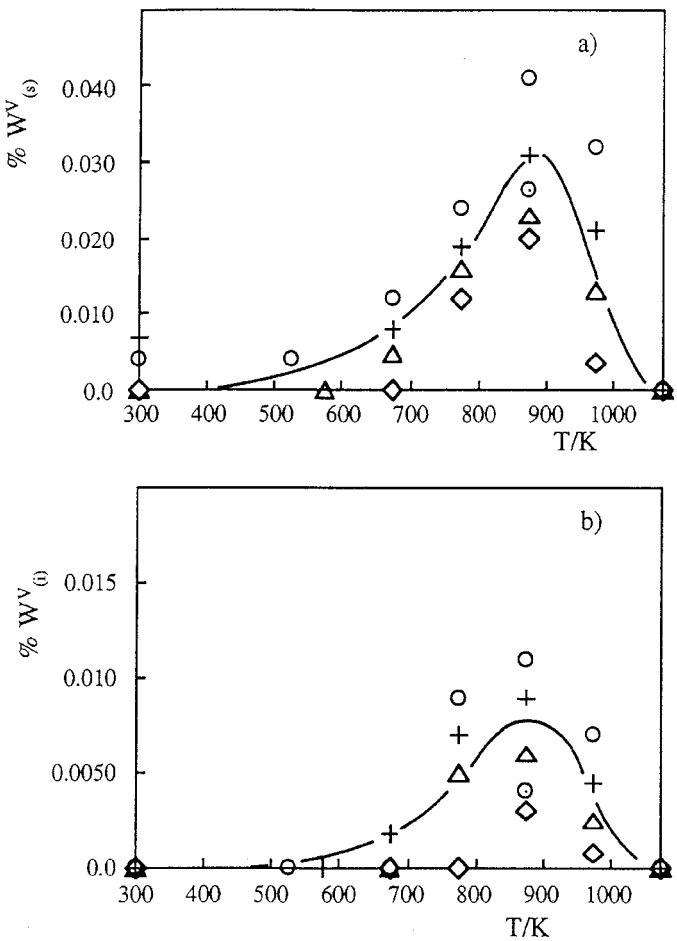

FIG. 9. Absolute concentration (at.%) of W^V substitutional (a) and interstitial (b) ions, detected by EPR as a function of the temperature of the treatment in air in TW0.1 (⊙), TW0.5 (+), TW1 (○), TW3 (△), and TW5 (◇).

treatment in oxygen or chlorine at 1000 K (37) and in anatase single crystal after irradiation at 77 K (38). Hence, when a strong Cr = O bond is formed, Cr^V is stabilized probably because of its high formal charge and very small ionic radius, i.e., its very high ionic potential.

After the thermal treatment in oxidizing atmosphere of TMo and TW, XRD indicated the M^{IV} oxidation at $T > 873$ K, whereas the more sensitive EPR technique showed that M^V formation started at 673 K. The EPR-detected M^V absolute concentration did not depend on the total M content because of the nonrandom distribution of M^{IV} ions. The EPR-detected M^V species are isolated species, namely those having no other magnetic ions (M^{III}, M^{IV}, and M^V) as nearest and possibly next-nearest neighbors. Magnetic susceptibility measurements indicate that in the more concentrated samples a large fraction of Mo^{IV} and almost all the W^{IV} ions are coupled. Hence the concentration of isolated M^{IV} ions, yielding M^V species after heating in air, is very low and almost independent on the total M content. The maximum concentration of EPR-detected M^V was lower in TW than in TMo (0.05% vs 0.14%), indicating a lower concentration of isolated M^{IV}, namely stronger metal–metal interactions, in TW than in TMo system. After thermal treatments in air at high temperature the W^V signal disappeared but the Mo^V concentration only decreased and MO_3 was segregated. Moreover, in the TMo samples reduced at 1073 K subsequent thermal treatments in oxidizing atmosphere restored isolated Mo^V species. These results indicate that segregation is more difficult in TMo than in TW.

Thermal treatment in oxidizing atmosphere also disclosed another difference between TMo and TW systems: interstitial Mo^V were absent, whereas W^V occupied both interstitial and substitutional sites. Interstitial W^V species could have formed either because some W^{IV} ions were displaced from a substitutional to an interstitial site during oxidation or because untreated samples already contained a small fraction of W^{IV} interstitial ions. The interstitial species are normally absent in TiO_2 and form only after special treatments. Interstitial Mo^V species in TiO_2 has been reported in MoO_2–TiO_2 prepared by burning a $MoOCl_2$–$TiCl_4$ mixture and subsequently reducing at low temperature (653 K) (26). Interstitial V^{IV} ions are formed in a single crystal of TiO_2 (25), by decreasing the temperature of the sample, sealed *in vacuo*, from 1173 to 873 K and by a subsequent quenching at RT. This observation argues in favor of W^{IV} ion displacement during oxidation, explaining why we detected no interstitial W^V in untreated samples.

The most noticeable difference between the TMo and the TW systems is their reduction process. Both XRD and EPR indicate that after the treatment in H_2 in the temperature range from 700 to 900 K, Mo^{IV} and Mo^V are reduced in solid solution to Mo^{III}, whereas in the TW system W^{IV} is not reduced to W^{III}. Because the reduction of isolated Mo^{IV}–Mo^{IV} pair yielded the dimeric Mo_2^{7+} species, the formation of this species in the dilute TMo sample provides evidence of the nonrandom distribution of Mo^{IV} ions. The isolated Mo^{IV}–Mo^{IV} pair has been identified in TiO_2 (39). Because the magnetic interactions are stronger in the TW system than in the TMo system, one would expect to find the analogous W^{IV}–W^{IV} pair in the TW 0.1 sample, but in reduced TW0.1 no dimeric W_2^{7+} formed. One explanation is that the redox properties of the two dimeric mixed valence species differ. Otherwise, isolated W^{III} ions might have escaped detection because magnetic and spectroscopic properties differ from those of Mo^{III}.

CONCLUSIONS

EPR and XRD characterization of TC, TMo, and TW solid solutions prepared *in vacuo* at 1173–1273 K indicates that the transition metal ions are incorporated in rutile as isolated and clustered Cr^{III}, Mo^{IV}, and W^{IV} and a small fraction as isolated Mo^V and W^V in substitutional sites.

The treatment in oxidizing and reducing atmosphere provides evidence that the stability of the transition metal ion incorporated in rutile varies. Whereas in TC the thermal treatments in air up to 1273 K yield no isolated Cr^V formation in solid solution, in TMo and TW the heating in air or in O_2 up to 1073 K causes the progressive oxidation $M^{IV} \rightarrow M^V \rightarrow M^{VI}$ and, at higher temperature, the segregation of MO_3. The oxidation process starts at 673 K, yielding isolated substitutional Mo^V ions and isolated interstitial and substitutional W^V ions. The maximum concentration of M^V is higher in TMo than in TW.

In TW and TMo after thermal treatment in H_2 up to 900 K, the reduction process differs: Mo^{IV} gives isolated and clustered Mo^{III} ions and Mo^{IV}–Mo^{IV} pairs yields Mo_2^{7+} species; and W^{IV} is not reduced to W^{III}. In both TW and TMo, temperatures higher than 900 K result in the segregation of the metallic phase. A subsequent heating of reduced TMo in O_2 reversibly restores isolated Mo^V ions.

REFERENCES

1. U. Gesenhues and T. Reutschler, *J. Solid State Chem.* **143,** 21 (1999).
2. M. Valigi, D. Gazzoli, M. Lo Jacono, G. Minelli, and P. Porta, *Z. Phys. Chem.* (*Neue Folge*) **132,** 29 (1982).
3. M. Valigi, S. De Rossi, D. Gazzoli, and G. Minelli, *J. Mater. Sci.* **20,** 71 (1985).
4. M. Valigi, D. Gazzoli, P. Natale, and P. Porta, *Gazz. Chim. Ital.* **116,** 391 (1986).
5. D. Cordischi, D. Gazzoli, and M. Valigi, *Gazz. Chim. Ital.* **113,** 579 (1983).
6. S. Ishida, M . Hayashi, Y. Fujimura, and K. Fujiyoshi, *J. Am. Ceram. Soc.* **73,** 3351 (1990).
7. D. Cordischi, M. Occhiuzzi, and R. Dragone, *Appl. Magn. Reson.* **16,** 427 (1999).
8. L. E. Halliburton, M. G. Jani, and R. B. Bossoli, *Nuclear Instrum. Methods Phys. Res. B* **1,** 192 (1984).

9. E. Serwicka, M. W. Schlierkamp, and R. N. Schindler, *Z. Naturforsch.* **36a,** 226 (1981).
10. S. A. Fairhurst, A. D. Inglis, Y. Le Page, J. R. Morton, and K. F. Preston, *Chem. Phys. Lett*. **95,** 444 (1983).
11. S. A. Fairhurst, A. D. Inglis, Y. Le Page, J. R. Morton, and K. F. Preston, *J. Magn. Reson.* **54,** 300 (1983).
12. Bor-Her Chen and J. M. White, *J. Phys. Chem.* **87,** 1327 (1983).
13. D. Cordischi, M. Valigi, D. Gazzoli, and V. Indovina, *J. Solid State Chem.* **15,** 82 (1975).
14. J. C. Evans, C. F. Relf, C. C. Rowlands, T. A. Egerton, and A. J. Pearman, *J. Mater. Sci. Lett*. **4,** 809 (1985).
15. A. Cimino, M. Lo Jacono, P. Porta, and M. Valigi, *Z. Phys. Chem.* (*Neue Folge*) **51,** 301 (1966).
16. T. T. Chang, *Phys. Rev.* **136,** A1413 (1964).
17. M. Che, G. Fichelle, and P. Meriaudeau, *Chem. Phys. Lett*. **17,** 66 (1972).
18. L. L. Van Reijen, Ph.D. thesis, Technische Hogeschool, Eindhoven, the Netherlands, 1964.
19. H. J. Gerritsen, S. E. Harrison, H. R. Lewis, and J. P. Wittke, *Phys. Rev. Lett*. **2,** 153 (1959).
20. W. D. Olsen, *Phys. Rev. B* **7,** 4058 (1973).
21. T. T. Chang, *Phys. Rev.* **147,** 264 (1966).
22. P. Meriaudeau, Y. Boudeville, P. de Montogolfier, and M. Che, *Phys. Rev. B* **16,** 30 (1977).
23. D. P. Madacsi, M. Stapelbroek, R. B. Bossoli, and O. R. Gilliam, *J. Chem. Phys.* **77,** 3803 (1982).
24. F. Kubek and Z. Sroubek, *J. Chem. Phys.* **57,** 1660 (1972).
25. H. J. Gerritsen and H. R. Lewis, *Phys. Rev.* **119,** 1010 (1960).
26. P. Meriaudeau, *Chem. Phys. Lett*. **72,** 551 (1980).
27. P. de Montgolfier, P. Meriaudeau, Y. Boudeville, and M. Che, *Phys. Rev. B* **14,** 1788 (1976).
28. P. de Montgolfier and Y. Boudeville, *Chem. Phys. Lett*. **37,** 97 (1976).
29. B. R. McGarvey *in* "Electron Spin Resonance of Metal Complexes" (Teh. F. Yen Ed.), Plenum, New York, 1969.
30. T. Shimizu, *J. Phys. Soc. Jpn.* **23,** 848 (1967).
31. F. E. Mabbs and D. Collison, *in* "Electron Paramagnetic Resonance of Transition Metal Compounds," Chap. 9, Elsevier, London, 1992.
32. D. Cordischi, M. Campa, V. Indovina, and M. Occhiuzzi, *J. Chem. Soc. Faraday Trans.* **90,** 207 (1994).
33. L. L. Van Reijen and P. Cossee, *Discuss. Faraday Soc*. **41,** 277 (1966).
34. J. H. Pifer, S. Ziemski, and M. Greenblatt, *J. Chem. Phys.* **78,** 7038 (1983).
35. D. Reinen, C. Albrecht, and U. Kashuba, *Z. Anorg. Allg. Chem.* **584,** 71 (1990).
36. Y. Ravi Sekhar and H. Bill, *J. Chem. Phys.* **82,** 645 (1985).
37. A. Lagendijk, R. J. Morel, M. Glasbeek, and J. D. W. Van Voorst, *Chem. Phys. Lett*. **12,** 518 (1972).
38. V. S. Grunin, I. B. Patrina, and G. D. Davtyan, *Sov. Phys. Solid State* **20,** 899 (1978).
39. P. Meriaudeau, B. Clerjaud, and M. Che, *J. Phys. Chem.* **87,** 3872 (1983).